Fe^{14+} and Fe^{15+} Spatial Distributions in a LHD Plasma Reconstructed from Multiple-Viewing-Chord EUV-Emission Observation*)

Jun YANAGIBAYASHI, Motoshi GOTO[1)], Chunfeng DONG[1)], Shigeru MORITA[1)] and Masahiro HASUO

Department of Mechanical Engineering and Science, Graduate School of Engineering, Kyoto University, Kyoto 606-8501, Japan

[1)]*National Institute for Fusion Science, Toki 509-5292, Japan*

(Received 22 December 2010 / Accepted 31 January 2011)

We have observed Fe^{14+} ($3s^2\ ^1S_0 - 3s3p\ ^1P_1$) and Fe^{15+} ($3s\ ^2S_{1/2} - 3p\ ^2P_{3/2}$) emissions from a LHD plasma with a space-resolved extreme-ultraviolet spectrometer. The observed intensity distributions against the viewing chord for the respective emissions are reconstructed to the emission flux distributions in the plasma against the normalized radius of the poloidal cross section with a maximum entropy method. Both of the emissions localize in the periphery region, and the Fe^{14+} emission is located outer side than that of Fe^{15+}. We calculate the charge state distribution of Fe ions against the normalized radius assuming the ionization equilibrium at the electron temperature and density, which are measured by a Thomson scattering method. The calculated result is consistent with the experimental one.

Keywords: highly charged ion, impurity, iron, EUV spectrum, spatial distribution, LHD plasma, periphery plasma

DOI: 10.1585/pfr.6.2402060

1. Inroduction

The transport study of the periphery region in a magnetically confined plasma for fusion research becomes important in a view point of the plasma performance improvement in addition to the confinement improvement. Impurity transport is one of major concerns [1]. Atoms of high Z elements like heavy metals are not fully ionized even in the core plasma. Such highly charged ions emit X ray and extreme ultraviolet (EUV) emission resulting in cooling of the plasma. Therefore, evaluation of the impurity ion density in the core plasma and its periphery region is demanded.

In the magnetically confined plasma, the electron temperature of the core plasma reaches keV range while that in the periphery region is in the order of 100 eV or less. As the result, charge states of impurity ions may largely vary from the core to periphery regions. Since the measured intensity of the emission from a plasma is integrated one along a viewing chord for the observation, one have to consider spatial distributions of charge states for the purpose of deducing the ion density. Furthermore, examination of the charge state distribution as functions of electron temperature and density is important for the validation of ionization equilibrium models.

In this paper, we report the spectroscopic observation of Fe^{14+} and Fe^{15+} emissions from a LHD plasma and the reconstruction of their spatial distributions from the observed emission intensities.

2. Experiment

Figure 1 (a) shows a schematic illustration of the plasma observation with a space-resolved EUV spectrometer having a laminar-type holographic grating [2]. The grating has a varied-line-spaced pattern with a central groove density of 1200 lines/mm. Emission from the plasma goes through a pin-hole slit, and then is incident on the grating at an incident angle of 87 degrees, and finally focused on an X-ray CCD detector ($26 \times 26\,\mu m^2$, 1024×225 pixels^2). Binning of 5×5 pixels^2 is done for the CCD image acquisition. As shown in the top view of Fig. 1 (a), the emission light is dispersed into 55 channels in the horizontal direction of the CCD while the vertical 205 channels correspond to the space-resolved observation through the pin-hole slit as shown in its side view. The corresponding viewing chords in the LHD poloidal cross section to the channels are shown in Fig. 1 (b).

Figure 1 (c) shows the two-dimensional image acquainted by the CCD detector for the LHD plasma (#95300), in which heating with ECH and two NBI beams start at $t = 3.3$ s. One of the NBI beams ends at $t = 4.85$ s and the other ends at $t = 5.3$ s. The exposure time of the

author's e-mail: hasuo@kues.kyoto-u.ac.jp

*) This article is based on the presentation at the 20th International Toki Conference (ITC20).

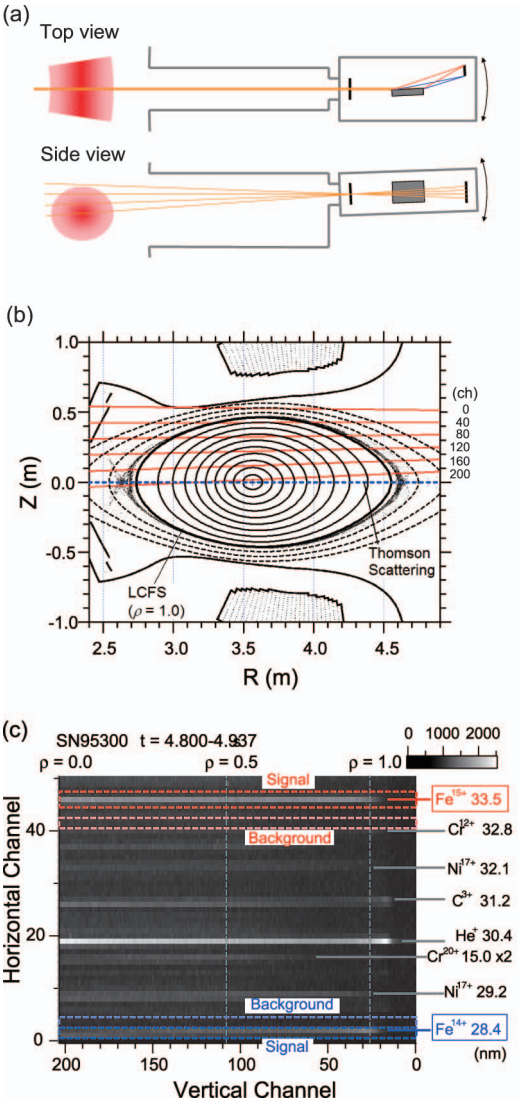

Fig. 1 (a) A schematic illustration of the top and side views of the space-resolved EUV spectrometer relative to a LHD plasma. The CCD horizontal channels direct the wavelength dispersion, while the vertical channels resolve the spatial distribution of the emission with the pin-hole-slit camera principle. (b) The LHD poloidal cross section and the viewing chords corresponding to the CCD vertical channels for the emission observation. (c) A CCD image of the observed emission through the spectrometer.

CCD is $t = 4.800$-4.937 s. The electron density and temperature at the plasma center measured by a Thomson scattering method [3] are 3×10^{19} m^{-3} and 1.1 keV, respectively, at the exposure time. The observed wavelength range is from 28 to 34 nm. Fe^{14+} ($3s^2\ ^1S_0 - 3s3p\ ^1P_1$, 28.4 nm) and Fe^{15+} ($3s\ ^2S_{1/2} - 3p\ ^2P_{3/2}$, 33.5 nm) emission lines are observed with several other impurity emission lines indicated in Fig. 1 (c).

Figure 2 shows the intensity distribution of the Fe^{14+} and Fe^{15+} emission lines against the CCD vertical channels obtained from the data shown Fig. 1 (c). The signals in two horizontal channels are summed for the Fe^{14+} emission, while those in three horizontal channels are summed for the Fe^{15+} emission. The signals of the region, where the line emissions are absent, are subtracted as the background (~ 630 counts/chennel). The used background regions are shown in Fig. 1 (c). Since the observed signal count is not so large, we estimate the magnitude of the error bars in Fig. 2 as the shot noise of the CCD photo-electrons, which is almost the same as the square root of the signal count including the background. We also assume that the spectrometer sensitivity is the same for all the viewing chords because the sensitivity of the CCD detector is rather uniform and the view angle of the CCD detector to the pinhole slit is within ± 2 degrees, which is small enough to assume the solid angles of all the viewing chords for the plasma to be the same. The observed intensity distribution of the Fe^{14+} emission has a peak in an outer region of the periphery plasma than that of the Fe^{15+} emission. The peak of the Fe^{14+} emission is broader than that of the Fe^{14+} emission.

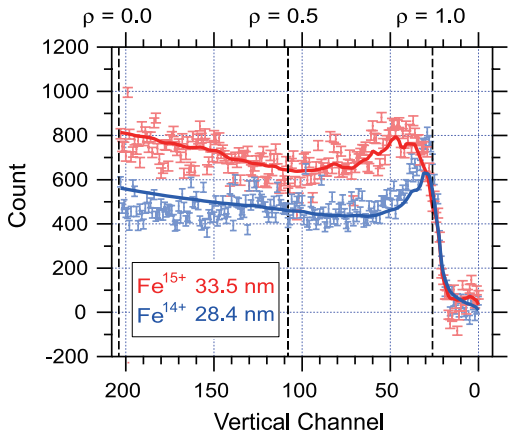

Fig. 2 Intensity distributions of the Fe^{15+} and Fe^{14+} emission against the CCD vertical channels. The normalized radius where the viewing chord is tangential to the magnetic surface is shown at the top label. The lines are the fitted results with a maximum entropy method.

3. Analysis

The intensity in each vertical channel shown in Fig. 2 is the line integrated one along the corresponding viewing chord. We reconstruct the distribution of the emission flux against the magnetic surface from the intensity distribution of Fig. 2. We assume that the emission flux has the same value at a magnetic surface having the same normalized radius because ions and electrons fast moves along a magnetic line, and then the plasma is homogeneous on the magnetic surface.

For the reconstruction, we express the observed intensity $S(i)$ at a viewing chord i, which is from 0 to 203, as

$$S(i) = \Sigma_j L(i, j)E(j) + d(i), \quad (1)$$

where $E(j)$ is the local emission flux at a magnetic surface

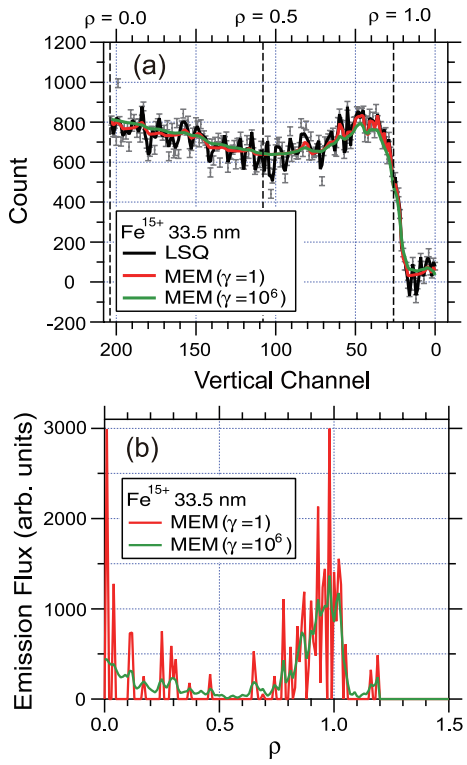

Fig. 3 (a) Intensity distributions of the Fe^{15+} emission against the CCD vertical channels and the fitted results with the least square and maximum entropy methods. (b) Emission flux distribution against the normalized radius obtained from the fit with the maximum entropy method.

number j. We divide the magnetic surfaces from 0 to 119 which correspond to the normalized radius, ρ, from 0.00 to 1.19. $L(i, j)$ is the length of a viewing chord i crossing a magnetic surface number j. $d(i)$ is the residual or error.

Firstly, we tried to deduce $E(j)$ with a least square method (LSQ); minimization of $D = \Sigma_i d(i)^2$. The fitted result to the distribution of the observed emission intensity is shown in Fig. 3 (a) by the black line and it shows unrealistic fluctuation on the channels. Furthermore, the scatter of the deduced $E(j)$ was found to be too large for the dependence on the normalized radius to be detected.

For the purpose of suppressing the scatter, we adopt a maximum entropy method (MEM) [4], in which the following evaluation function is minimized.

$$Q = \gamma H - D, \tag{2}$$

where H is the entropy defined as

$$H = -\Sigma_j \frac{E(j)}{\Sigma_j E(j)} \ln \frac{E(j)}{\Sigma_j E(j)}, \tag{3}$$

and γ is the regularization parameter. It is noted that $E(j)$ is limited to be positive from eq. (3) even in the presence of the scatter.

The entropy is an indication of the smoothness of $E(j)$. When γ is small, $E(j)$ has large scatter as seen in Fig. 3 (b) (the $\gamma = 1$ case) but its localization around $\rho =$

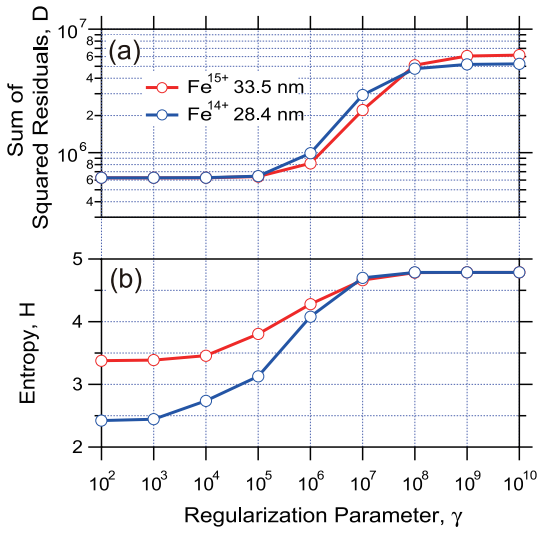

Fig. 4 (a) Sum of the squared residuals and (b) entropy as a function of γ in the maximum entropy method.

1 is clearly seen. At a very large γ, $E(j)$ may become too smooth to reproduce $S(i)$. Figures 4 (a) and (b) show D and H, respectively, as a function of γ for both the Fe^{14+} and Fe^{15+} emissions. To obtain a relatively large H without a large increase in D, we choose γ to be 10^6. The results of the fit are shown in Figs. 3 (a) and (b) by the green lines. It is noted that presence of the emission flux around $\rho = 0$ and $\rho > 1.1$ are due to the limitation of $E(j)$ in the MEM calculation. The fitted results are also shown in Fig. 2 for both the emissions.

4. Results and Discussion

Figure 5 (a) shows thus converted Fe^{14+} and Fe^{15+} emission flux distributions against the normalized radius. We assume the system sensitivities for the Fe^{14+} and Fe^{15+} emissions to be the same because their wavelengths are close to each other [5]. The absolute sensitivity of the system, however, is not known at present, and then the unit in Fig. 5 (a) is arbitrary. The Fe^{15+} emission distribution has a sharp peak in an outer region of the periphery plasma than that of the Fe^{14+} emission.

Figures 5 (b) and (c) show the distributions of the electron density and temperature, respectively, measured by the Thomson scattering method along the dashed line in Fig. 1 (b). The lines in Figs. 5 (b) and (c) are the fitted curves to the experimental data points used for the calculation below.

We estimate the Fe^{14+} and Fe^{15+} densities in the ground state, $n_i{}^q(j)$, from $E^q(j)$ with an equation of

$$n_i{}^q(j) = \frac{E^q(j)}{R^q(T_e(j))n_e(j)}, \tag{4}$$

where $n_i{}^q(j)$ is the ion density of a charge state q in the ground state. $T_e(j)$ and $n_e(j)$ are the electron temperature and density, respectively. $R^q(T_e(j))$ is the emission rate co-

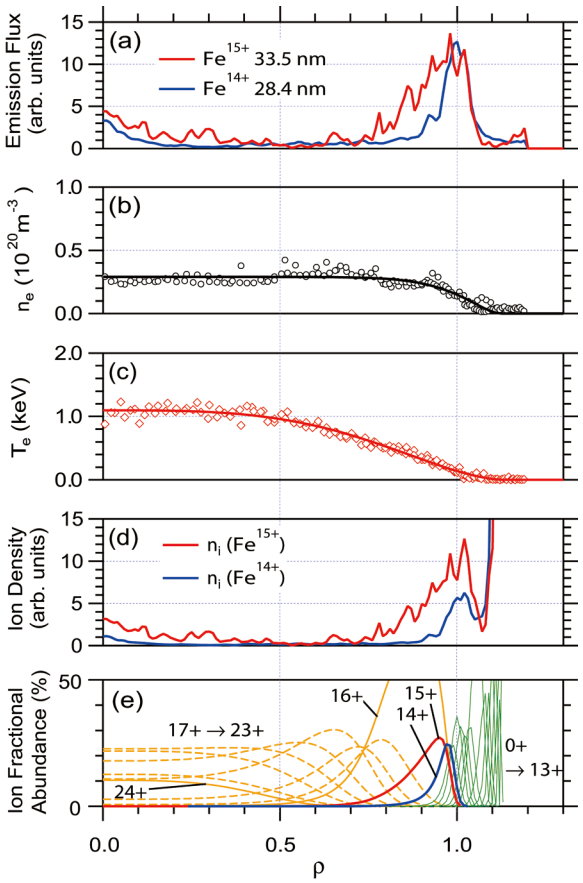

Fig. 5 (a) Fe^{14+} and Fe^{15+} emission flux against the normalized radius. The electron density (b) and temperature (c) distributions measured by a Thomson scattering method along the dashed line in Fig. 1 (b). (d) Density distributions of Fe^{14+} and Fe^{15+} ions calculated from the emission flux distributions. (e) Charge state distributions of Fe ions estimated from the ionization equilibrium.

efficient, which is shown in Fig. 6, estimated with the Flexible Atomic Code [6] and a collisional-radiative model calculation assuming a steady state [7]. The estimated density distributions are shown in Fig. 5 (d). The sudden increase at $\rho > 1.05$ is artifact because the electron density becomes very small there. The treatment for the data background and scatter in Fig. 3 and Fig. 5 (a) may be insufficient. Its improvement is, however, very difficult in the present status of the experiment and analysis.

We also calculate the charge state distribution of Fe

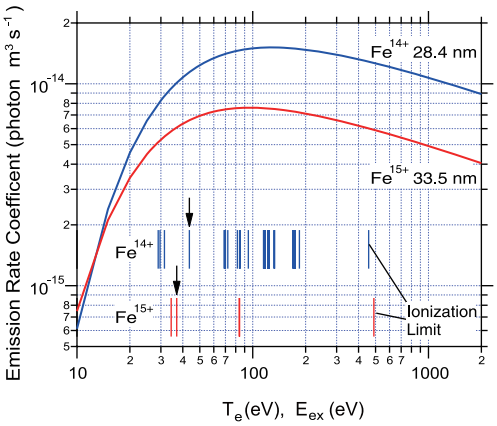

Fig. 6 Emission rate coefficients for the observed Fe^{14+} and Fe^{15+} emissions as a function of the electron temperature. Excitation energies of the Fe^{14+} and Fe^{15+} ions are also shown. The upper levels of the observed emissions are indicated by the arrows.

ions against the normalized radius assuming the ionization equilibrium at the electron temperature and density [8]. From the ionization rate of Fe, the equilibration time is estimated to be in the order of 10 μs. The experimental Fe ion density distributions are found to be well reproduced by the calculated profiles of the respective ion fractional abundances.

Acknowledgement

The authors thank all members of LHD experiment group for their technical supports. This work was partly carried out under the LHD project financial supports (NIFS10ULPP010 and KKGP013).

[1] S. Morita *et al.*, Plasma Science and Technology **11**, 402 (2009).
[2] C.F. Dong *et al.*, Rev. Sci. Instrum. **81**, 033107 (2010).
[3] K. Narihara, I. Yamada, H. Hayashi and K. Yamauchi, Rev. Sci. Instrum. **72**, 1122 (2001).
[4] N. Iwama *et al.*, J. Appl. Phys. **52**, 5466 (1981).
[5] M.B. Chowdhuri *et al.*, Rev. Sci. Instrum. **78**, 023501 (2007).
[6] M.F. Gu, Astrophys. J. **582**, 1241 (2003).
[7] T. Fujimoto, *Plasma Spectroscopy*, (Clarendon Press, Oxford, 2004).
[8] M. Arnaud and J. Raymond, Astrophys. J. **398**, 394 (1992).